Applied Catalysis B: Environmental 148–149 (2014) 281–287

Contents lists available at ScienceDirect

Applied Catalysis B: Environmental

journal homepage: www.elsevier.com/locate/apcatb

Facile synthesis of porous microspheres composed of TiO_2 nanorods with high photocatalytic activity for hydrogen production

Kai Yan, Guosheng Wu, Cody Jarvis, Jiali Wen, Aicheng Chen *

Department of Chemistry, Lakehead University, 955 Oliver Road, Thunder Bay P7B 5E1, ON, Canada

ARTICLE INFO

Article history:
Received 9 August 2013
Received in revised form 6 October 2013
Accepted 1 November 2013
Available online 10 November 2013

Keywords:
Photocatalysis
TiO_2 microspheres
Nanorods
High surface area
Hydrogen production

ABSTRACT

A facile, high-yield and reproducible hydrothermal route was developed to synthesize novel well-knit (i.e., solid and compacted) and porous anatase TiO_2 microspheres, consisting of morphologically controlled and uniform TiO_2 nanorods. Field emission scanning electron microscopy (FE–SEM) and transmission electron microscopy (TEM) revealed that the resulting TiO_2 microspheres exhibited a nanoporous structure that was formed by the self-assembled accumulation of uniform nanorods, which is reported here for the first time. The effect of the surfactant type, surfactant amount and other additives such as urea and water on the formation of the microspheres was investigated. X-ray diffraction and N_2 adsorption–desorption characterization showed that the synthesized TiO_2 microspheres exhibited a high degree of crystallinity with a high surface area (~103.9 m^2/g), which was twice larger than that of commercial P25. The synthesized TiO_2 microsphere photocatalysts also exhibited superior photocurrent density with a 4.8-fold improvement in photocurrent over the commercial P25. Additionally, these TiO_2 microspheres showed good performance in the generation of hydrogen.

1. Introduction

The synthesis of TiO_2 nanocrystals with well-defined textures has attracted extraordinary attention and is critical for elucidating the surface structures of materials toward the determination of their properties [1–3]. Anatase TiO_2 constitutes one of the most studied oxide semiconducting materials, and has been widely utilized in photocatalysis, the photosplitting of water, dye-sensitized solar cells, photochromic devices, and gas sensing [4–6]. These applications strongly depend on its surface properties. Over the last a few decades, great efforts have been expended in the synthesis of anatase TiO_2 single crystals with a high percentage of {0 0 1} facets, which are formed utilizing toxic HF as the morphology-directing agent in a TiF_4 aqueous solution [7–10], or via a non-aqueous synthetic route [11,12]. The resulting TiO_2 with well-defined {0 0 1} facets is particularly useful for solar energy applications [13,14].

Recently, significant research efforts have been allocated to the design of TiO_2 microspheres with desired functionality, due to their unique material properties (e.g., high surface area, good chemical and thermal stability, excellent electronic and optical properties). These features render them greatly promising for applications such as photocatalysis, solar-cells, lithium-ion batteries, catalyst supports, and heterogeneous catalysts [15–17]. Templating methods have been widely employed to generate multiple hollow structures [18,19]. A large number of studies involving conventional templating methods have focused on interactions between surfactants and titanium species in the realization of specific morphologies [20,21]. It has been concluded that the surfactant-titanium precursors spontaneously organize through the interactive matching of organic and inorganic components. With careful control of the self-assembly and titanium condensation rate, it is possible to control the dimensions, crystal structures and morphologies of the spheres [20–25]. Zhang et al. reported the formation of hollow mesoporous TiO_2 spheres using titanium butoxide as the precursor in the presence of concentrated NH_3H_2O [24]. Recently, Gu et al. reported the synthesis of mesoporous hollow spherical TiO_2 via hydrothermal silica etching [26]. More recently, Snaith et al. have reported the synthesis of mesoporous TiO_2 single crystals using a mesoporous silica template in conjunction with a TiF_4 precursor [27]. However, as yet, reports are lacking of describing the synthesis of compacted and nanoporous TiO_2 microspheres. Herein, we have developed a facile, high-yield and reproducible hydrothermal route to synthesize well-knit and nanoporous anatase TiO_2 microspheres with a controllable texture, good structural stability, and high surface area. To the best of our knowledge, this is the first report on the construction of solid and porous anatase TiO_2 microspheres with uniform TiO_2 nanorods. The high surface areas of the resulting TiO_2 microspheres exhibited superior photocatalytic properties, where their photocurrent densities demonstrated a 4.8-fold improvement over those of commercial P25. In addition, the synthesized TiO_2

* Corresponding author. Tel.: +1 807 3438318; fax: +1 807 346 7775.
E-mail address: aicheng.chen@lakeheadu.ca (A. Chen).

0926-3373/$ – see front matter © 2013 Elsevier B.V. All rights reserved.
http://dx.doi.org/10.1016/j.apcatb.2013.11.003

microspheres displayed excellent performance in the hydrogen production.

2. Experimental methods

2.1. Chemicals

Poly(propylene glycol)-block-poly(ethylene glycol)-block-poly(propylene glycol) (P123, average molecular weight ~2000), hexadecyltrimethylammonium bromide (CTAB, BioUltra, ≥99.0%), titanium(IV) chloride ($TiCl_4$, ≥99.0%), urea (powder, ACS reagent), absolute ethanol (99.98%, GC) were purchased from Sigma-Aldrich. P25 (titanium dioxide nanoparticles) was purchased from Degussa. Pure H_2O was obtained from a NANOpure® Diamond TM UV ultrapure water purification system. All chemicals were used directly without further treatment.

2.2. Synthesis of TiO_2 microspheres

TiO_2 microspheres were synthesized in the presence of P123 surfactant, where the typical procedure was as follows: different amount of P123 surfactant, varying from 0.0 to 4.0 g, were dissolved into 40 mL of ethanol under stirring for 1 h. Subsequently, 1.0 mL of $TiCl_4$ was rapidly transferred under an argon environment and continuous stirring conditions. Subsequently, 7.0 g of urea and 15 mL of water were added to the solution, respectively, and stirred further for 30 min. The resulting solution was transferred into a 150 mL container and placed in an oven for hydrothermal treatment at 110 °C for 20 h. Following the hydrothermal treatment, the formed gel was centrifuged for 30 min, rinsed with pure water and dried at 110 °C for 24 h in an oven. Finally, the dried gel was calcinated under 450 °C for 3 h in a furnace. The TiO_2 microspheres prepared in the presence of 1.0, 2.0 and 4.0 g P123 surfactant were abbreviated as TiO_2-1, TiO_2-2, TiO_2-4, respectively.

2.3. Catalyst characterization

The resulting samples were examined with a TEM (JEOL-2010 at 200 KV) to investigate their structural features. Field Emission Scanning Electron Microscope (FE–SEM) was performed with a Hitachi SU-70 at 10.0 kV in order to elucidate the morphologies of the samples. The cross-section of the samples was prepared by Hitachi ion milling system (IM4000) and characterized using SEM (S4800 at 1.0 kV). Thermogravimetric Analysis (TGA) was operated under a N_2-enviroment using STA 449 F3 (Netzsch Pvoteus Thermal Analysis). Powder X-ray diffraction (XRD) patterns for the crystalline phase analysis were collected using a Phillips PW 1050-3710 with Cu $K\alpha_1$ of 1.54060 Å as the radiation source. Data was collected in the range of 30°–70° 2θ with a step width of 0.01°/2θ. The particle sizes (L) for each sample were calculated using the Scherrer Equation (1), where λ corresponds to the Cu $K\alpha$ radiation, and β is the full width at half-maximum (FWHM) for a reflection maximum, located at 2θ).

$$L = \frac{0.9\lambda}{\beta\cos\theta} \quad (1)$$

Nitrogen adsorption–desoprtion was measured using a NOVA 2020 sorption analyzer (Quantachrome) at 77 K, and the samples were activated under a vacuum of 0.01 mbar at 200 °C for 3 h prior to the measurements. The surface area was calculated from the adsorption isotherm. Pore size distributions were calculated using the Barrett–Joyner–Halenda (BJH) method, employing models for nitrogen adsorption at 77 K, for both the adsorption and desorption branch of the isotherms. The total volume (Vp) was estimated from the adsorbed amount at a relative pressure P/P_0 of 0.995.

2.4. Linear voltammograms and transient photocurrent-time profiles

Linear voltammograms were recorded using a PGZ 301 VoltaLab. A three-electrode cell was utilized comprising an Ag/AgCl reference electrode, a Pt wire coil as the counter electrode and the prepared Ti/CP, Ti/CP/P25 and Ti/CP/TiO_2 microspheres as the working electrodes, where Ti was used as the substrate and CP denotes a carbon paste thin film. To fabricate the Ti/CP/P25 and Ti/CP/TiO_2 electrodes, the same amount (~10 mg) of P25 and TiO_2 microspheres were uniformly immobilized on the Ti-supported CP thin film. A Dymax Cure Spot 50 (main line of emission, 365 nm) with an intensity of ~2.0 mW/cm^2 was employed for irradiation. Data acquisition and analysis were performed using VoltMaster 4 software, and all experiments were carried out at room temperature, 20 ± 2 °C.

2.5. Hydrogen generation tests

H_2 generation experiments were performed by dispersing 20 mg of the photocatalyst (Pt supported on the synthesized TiO_2 microspheres) in a 10 mL methanol solution (10 vol%), which served as a sacrificial electron donor, where the photocatalyst was prepared by traditional impregnation and then reduced by the ammonia format solution (1 M). The reactant solutions were evacuated several times in order to completely remove the internal atmosphere prior to irradiation under a 300 W Xenon arc lamp and a water filter (Oriel System). The reactant solution was maintained at room temperature during the reaction by means of a cooled water flow. The evolved gases were analyzed via gas chromatography (GC, Shimadzu GC-2014, Column: Silica gel, thermal conductive detector (TCD), the column temperature was raised from 40 to 250 °C at a heating rate of 3 °C/min; the injector temperature was set at 70 °C, with a heating velocity of 25 °C/min; the sampling volume was 0.5 mL).

3. Results and discussion

3.1. Characterization of TiO_2 microspheres

In an initial investigation, we focused on the fabrication of TiO_2 microspheres in the presence of 2.0 g of P123 surfactant under mild conditions. The morphologies and structure of the obtained TiO_2 particles were initially characterized by FE–SEM (Fig. 1a–d). Fig. 1a depicts a typical spherical morphology with relatively uniform dispersion. Dimensionally, some of the microspheres were well organized (Fig. 1b). The average diameter of the TiO_2 microspheres was ~1 μm (Fig. 1c), which were cumulatively built up from uniform TiO_2 nanorods, as shown in Fig. 1d. Subsequently, we focused on the influence of different amount of the P123 surfactant on the texture of the resulting TiO_2 particles. For the initial photocatalyst (TiO_2-1), the typical TiO_2 microsphere diameter was ~2.8 μm (Fig. 1e), where the microspheres were also cumulatively built up from TiO_2 nanorods (Fig. 1f). When the amount of the P123 surfactant was further increased to 4.0 g (TiO_2-4), the diameter of the synthesized TiO_2 microspheres was reduced to ~0.6 μm in diameter (Fig. 1g), and was comprised of much shorter TiO_2 nanorods (Fig. 1h). This confirmed that the 2.0 g amount of P123 surfactant better facilitated the formation of TiO_2 microspheres with highly uniform and longer TiO_2 nanorods. Overall, it indicated that a well-defined amount of the P123 surfactant was beneficial for the formation of high quality TiO_2 microsphere structures with tailorable diameters and morphologically controllable nanorods, which were further definitively confirmed by our TEM analysis.

In a further design, we turned our attention to the effect of surfactants. Another common surfactant (CTAB), which has been used

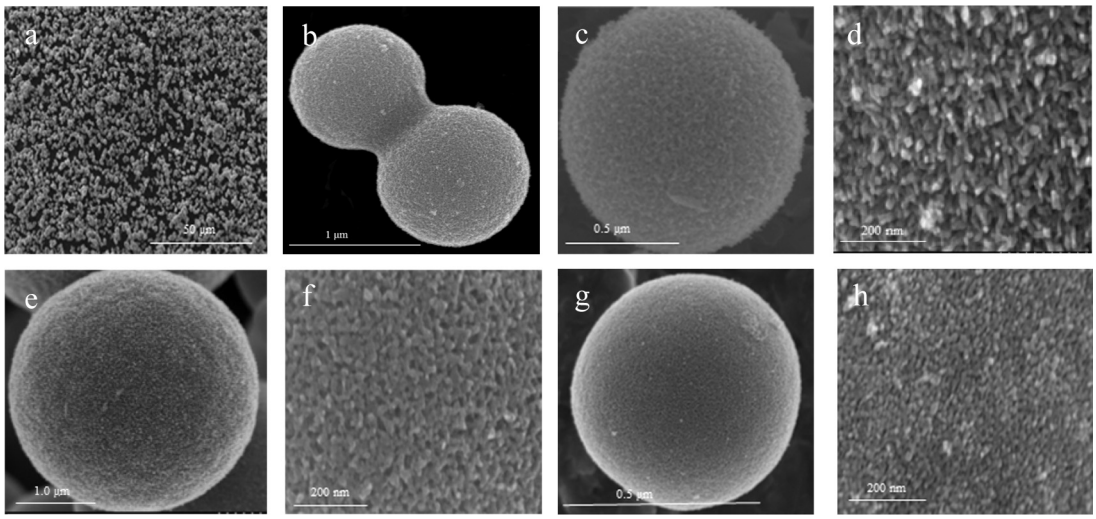

Fig. 1. FE–SEM images of the formed TiO_2 microspheres in the presence of different amount of surfactant: (a–d) 2.0 g; (e and f) 1.0 g; (g and h) 4.0 g.

in the synthesis of mesoporous SiO_2 [20,21], was also utilized in this study for comparison, and FE–SEM was again employed to investigate the morphology of the resulting TiO_2 particles, as shown in Fig. S1 (see Appendices A and B). The FE–SEM images (Fig. S1) revealed that the resulting TiO_2 microspheres were irregular with diameters of ~3.5 μm. High magnification FE–SEM images revealed that the microspheres were composed of TiO_2 nanoparticles. Alternatively, these results further confirmed that the P123 surfactant was superior for the formation of regular microspheres composed of uniform nanorods. This could be attributed to the fact that the P123 surfactant, tri-block copolymer, possesses relatively large hydrophobic tails and can form a more densely packed micelle structure than the CTAB surfactant [15,20,21].

In proceeding with the study of the internal structure of the resulting microspheres, a typical TiO_2-2 microsphere was cleaved (Fig. 2). Interestingly, we found a well-knit and highly porous interior that consisted of densely packed nanorod subunits as seen in Fig. 2a. The above results have shown that well-knit and porous TiO_2 microspheres comprised of aggregated nanorods with well-dispersed uniformity were successfully fabricated in the presence of P123 surfactant.

The solid interiors of the representative microspheres (TiO_2-2 and TiO_2-4 photocatalysts) prepared by P123 surfactant were further characterized by TEM, as shown in Fig. 3, which indicated a well-defined net composed of highly ordered nanorods. From the TEM images (Fig. 3a) of the fabricated TiO_2-2 microspheres, it can be seen that the subunits were wedge-shaped nanorods (Fig. 3b), which were ~21.5 nm in length and ~11.3 nm in diameter, and thus imparted a subtle curvature to facilitate the construction of the solid spherical structure (Fig. 3a). A selected area electron diffraction (SAED) pattern (inset in Fig. 3b) indicated the *d* values of 0.342 nm of the plane (1 0 1) of anatase TiO_2, which is further confirmed by the high-resolution TEM image presented in Fig. 3c. When the amount of the P123 surfactant was increased to 4.0 g (TiO_2-4), the TEM image (Fig. 3d) indicated the formation of smaller sized (~0.6 μm) TiO_2 microspheres. It can be seen that the subunits were composed of nanorods (Fig. 3e and f) with dimensions of ~12.3 nm in length and ~6.5 nm in diameter, which is consistent with the aforementioned FE–SEM images (Fig. 1h). A selected area electron diffraction (SAED) pattern (inset in Fig. 3e) and the high-resolution TEM image (Fig. 3f) collectively showed the *d* value of 0.349 nm of the plane (1 0 1) of the formed anatase TiO_2 microspheres.

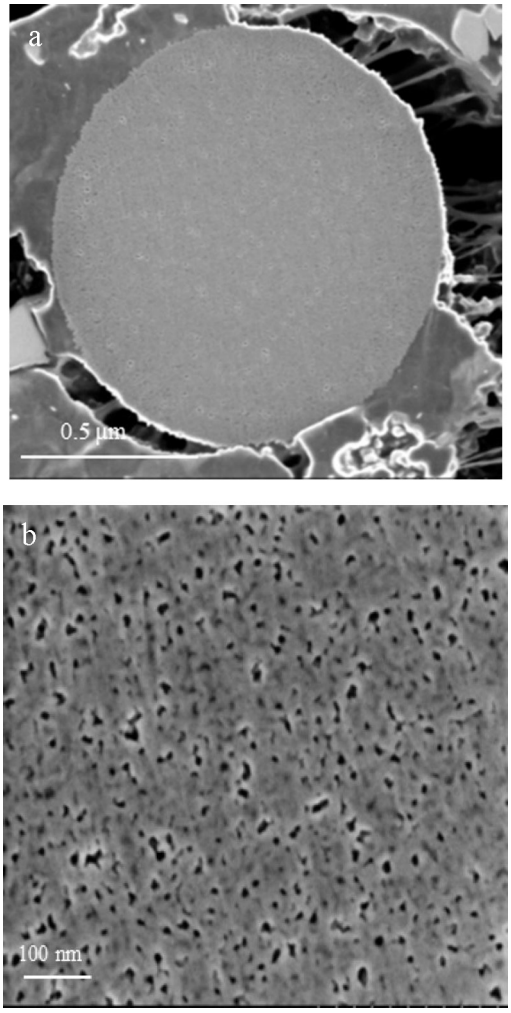

Fig. 2. SEM images of the cross-section of a representative cleaved TiO_2-2 microspheres recorded at the magnification of 35,000 (a) and at a high magnification of 150,000 (b).

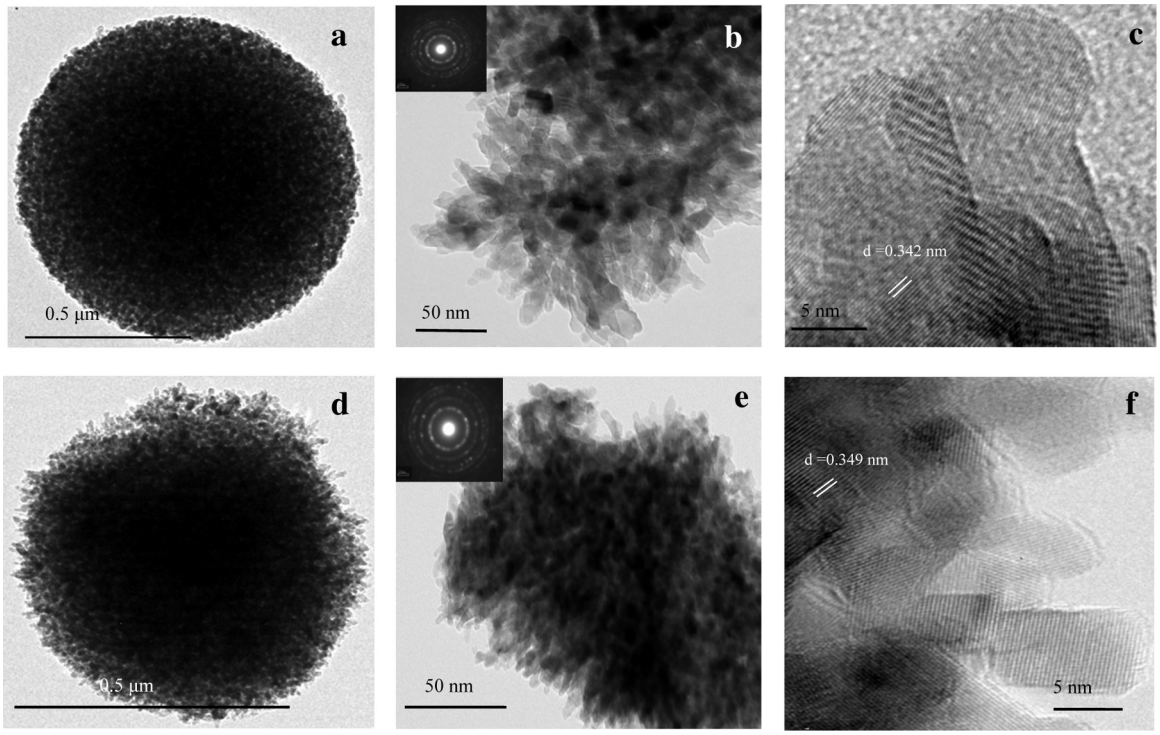

Fig. 3. TiO_2 microspheres prepared in the presence of different volumes of P123 surfactant: (a–c) TEM images of TiO_2-2; (d–f) TEM images of TiO_2-4 with inset of SAED analysis.

The crystal phase of the calcinated product was further determined by XRD analysis (Fig. S2). The diffraction peaks in the XRD pattern can be unambiguously assigned to the pure anatase TiO_2 phase (JCPDS card no. 01-071-1168; Tetragonal; $a = b = 3.7971$ Å, $c = 9.5790$ Å) with high crystallinity. Mean sizes of 0.269 nm (Fig. S2a), 0.272 nm (Fig. S2b) and 0.273 nm (Fig. S2c) were calculated from the plane (1 0 1) of the anatase TiO_2 based on the Scherrer Equation, respectively.

The thermal decomposition of pre-synthesized precursor nanostructures is an attractive way to remove the surfactant, and to obtain tailored metal-oxide nanostructures [28,29]. TGA was further employed to study the thermal stability of the formed gel, as shown in Fig. 4. The TGA curve *a* revealed that the precursor of the TiO_2 microspheres underwent four terraces during the increase of the temperature from 20 to 800 °C. The gel initially underwent a slight weight loss prior to reaching 200 °C, corresponding to the loss of physisorbed water molecules. The second terrace appeared between 200 and 300 °C, which was likely due to the removal/decomposition of the urea that remained in the sample [30]. The significant weight loss (ca. 40 wt%), was located between 300 and 500 °C, which might be attributed to the elimination of the P123 surfactant. Beyond 450 °C, a relatively stable terrace appeared, indicating that no further structural change occurred and that a stable metal oxide phase was obtained. In comparison, the TGA curve *b* (in Fig. 4) of the TiO_2 samples following calcination at 450 °C for 3 h displayed high stability in the investigated temperature range from 100 to 800 °C, confirming that the calcined temperature of 450 °C was optimal for the removal of the P123 surfactant and thus, for the formation of TiO_2 microspheres.

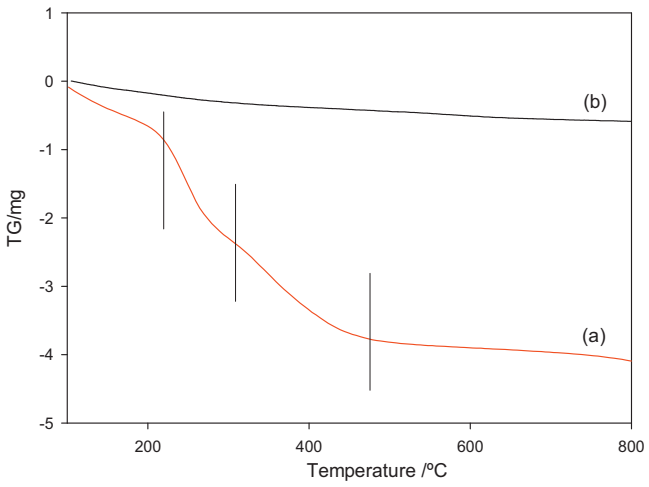

Fig. 4. TG analysis of the TiO_2 precursor gel prior to (a) and following calcination at 450 °C for 3 h (b).

The N_2 adsorption–desorption isotherm of the as-obtained anatase TiO_2 microspheres is shown in Fig. S3. Nitrogen sorption isotherms of the well-knit anatase TiO_2 microsphere (TiO_2-2 and TiO_2-4) were a characteristic type IV curve with the hysteresis loop at the evident capillary condensation steps at a relative pressure (P/P_0) in the range of 0.4–0.7, which demonstrated the presence of a porous structure in these materials. This is also consistent with the FE–SEM image of the internal structure (Fig. 2b). The numeric value analysis was summarized and depicted in Table 1. A relatively high BET specific surface area was achieved in the presence of the P123 surfactant. The TiO_2-2 photocatalyst possessed a maximum surface area of 103.9 m^2/g (Entry 3). Without the presence of the P123 surfactant (Entry 1), a much lower surface area of 17.4 m^2/g was obtained, which strongly argued for the crucial role of the P123 surfactant in the enhancement of the surface area and the resultant porosity. The value of the surface area of TiO_2-2 (Entry 3) was approximately twice of the commercial P25. In addition, there was an enhancement in the mesoporous as well as microporous volumes in association with increased amounts of the P123 surfactant.

Table 1
BET analysis of the resulting TiO_2[a].

Entry	P123 amount (g)	Crystal size[b] (nm)	S_{BET} (m^2/g)	V_{meso} (cm^3/g)	r_{meso} (nm)	V_{micro} (cm^3/g)	r_{micro} (nm)
1	0.0	0.202	17.4	0.171	4.41	0.110	1.28
2	1.0	0.269	79.0	0.145	4.38	0.101	1.26
3	2.0	0.272	103.9	0.210	4.39	0.148	1.32
4	4.0	0.273	92.0	0.242	4.37	0.152	1.26

[a] Other synthesis conditions were identical.
[b] Crystal size was calculated from XRD patterns using the Scherrer equation.

A mesoporous volume of 0.210 cm^3/g and a microporous volume of 0.148 cm^3/g were observed in the case of TiO_2-2 (Entry 3), while the values obtained were a mesoporous volume of 0.242 cm^3/g and a microporous volume of 0.152 cm^3/g, for the TiO_2-4 photocatalyst (Entry 4). As seen in Table 1, the surface area of the formed microspheres was slightly decreased with the increase of the P123 surfactant from 2.0 to 4.0 g. This is likely due to the fact that the higher amount of surfactant (e.g., 4.0 g) would result in more condensed microspheres composed of the smaller size of nanorods as demonstrated by the FE–SEM (Fig. 1) and TEM images (Fig. 3).

In the course of the synthesis, ethanol was employed as the solvent; urea and water were used as the additives for hydrolization; and the P123 surfactant served as the structure directing agent for the formation of the well-knit microspheres as illustrated in Scheme 1. To investigate the roles of the surfactant P123 and the additives (urea and water) in the synthesis procedure, three parallel tests were carried out under the same conditions. No gel was formed in the absence of water. Hence, the addition of water was responsible for the hydrolysis and the subsequent condensation of the intermediates [15], as illustrated in Scheme S1. The addition of the P123 surfactant was found to play a critical role in the formation of the microsphere structure. In the absence of the P123 surfactant, no regular spheres were observed, as shown in Fig. S4a. Additionally, only a ~40% yield of TiO_2 was obtained. In the presence of the P123 surfactant, the $TiCl_4$ precursor was initially internally dispersed, hydrolyzed into a TiO_2 gel, assembled and then grown along the P123 surfactant micelle. Following the removal of the P123 surfactant, the well-knit TiO_2 microspheres are produced. Moreover, in the presence of the P123 surfactant, a high yield of TiO_2 (>95%) was achieved. The addition of urea served a double role as it not only promoted the hydrolysis and condensation steps due to its weak basicity of urea, but was also beneficial for the formation of the porous texture via the release of ammonia [31]. In the absence of urea, aggregated TiO_2 plates and irregular TiO_2 particles (Fig. S4b) were produced under the same experimental conditions.

3.2. Photocurrent measurements

Fig. 5 presents the linear voltammograms (LVs) of the fabricated TiO_2 microspheres and P25 versus the electrode potential recorded in 0.5 M Na_2SO_4 solution in the absence of light irradiation (A) and under the UV–visible light irradiation (B). As shown in Fig. 5A, without the light irradiation, the Ti/CP/TiO2 microspheres (Curve *c*–*e*) and the Ti/CP/P25 (Curve *b*) electrode exhibited a slightly higher current than the Ti/CP electrode. However, the LVs of all the Ti/CP/TiO_2 microspheres and the Ti/CP/P25 electrode were almost identical. Upon the UV–visible light irradiation, no obvious change was observed for the bare Ti/CP electrode (Curve *a* of Fig. 5B). In contrast, significant increase of the photo current occurred in the following order: Ti/CP/P25 ≪ Ti/CP/TiO_2-4 < Ti/CP/TiO_2-1 < Ti/CP/TiO_2-2. For instance, at the electrode potential 1.0 V, the net photocurrent of the TiO_2-2 microspheres was calculated by subtracting the photocurrent shown in Fig. 5B from the background current displayed in Fig. 5A to be 95.4 μA/cm^2, which is 4.8 times higher than that of the commercial P25 (20.0 μA/cm^2). This might be attributed to the high surface area, as well as the uniform and long nanorods. The difference in the photocurrent density of the different TiO_2 microspheres was likely due to their internal structure, where the length of the nanorods and the resulting surface areas might play a crucial role. Alternatively, this demonstrated that the separation rate of photogenerated holes and electrons increased significantly following the formation of the microspheres. More photogenerated electrons collected from the TiO_2 microsphere suggested that more photogenerated holes survived from recombination or from the longer lifetime that the holes had.

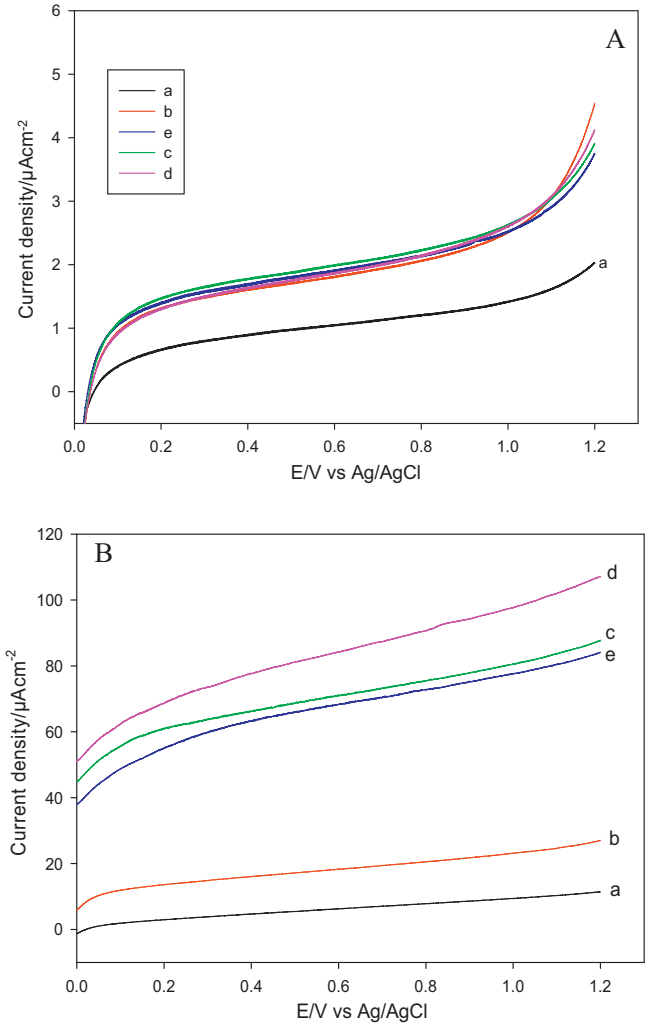

Fig. 5. Linear voltammograms of the fabricated Ti/CP/TiO_2 microspheres in the absence (A) and presence (B) of the UV-visible irradiation; Ti/CP (a); and Ti/CP/P25 (b); Ti/CP/TiO_2-1 (c); Ti/CP/TiO_2-2 (d) and Ti/CP/TiO_2-4 (e) recorded in 0.1 M Na_2SO_4 at the scan rate of 20 mV/s.

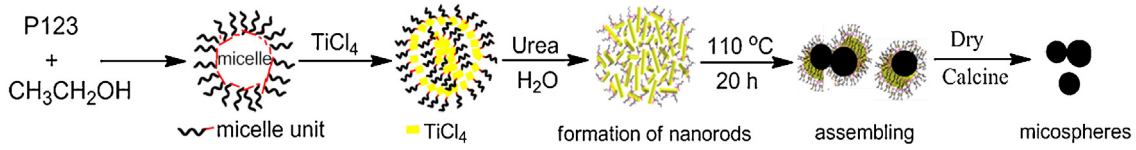

Scheme 1. Schematic diagram for the synthesis of TiO_2 microspheres.

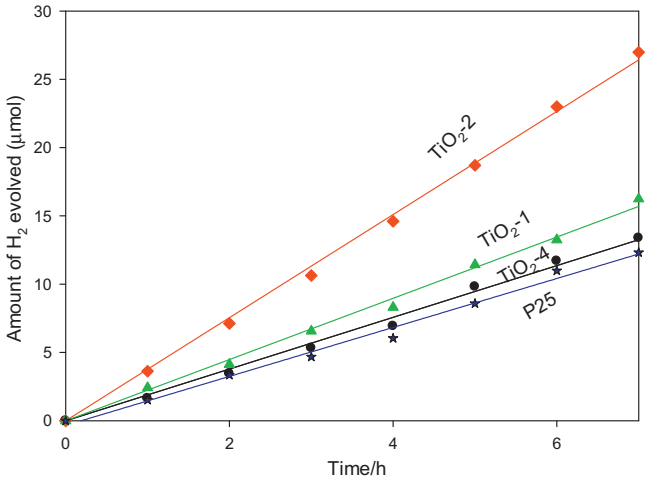

Fig. 6. Hydrogen production of the synthesized TiO_2 microspheres and P25.

3.3. Hydrogen generation tests

We further investigated the photocatalytic activity of the synthesized nanoporous TiO_2 microspheres and the commercial P25 toward hydrogen production. Fig. 6 presents the time profile of H_2 evolution on the photocatalysts at 10 wt% Pt supported on the TiO_2 microspheres and P25 under the UV light irradiation. The resulting TiO_2 microspheres displayed UV-light induced H_2 generation. The amount of hydrogen evolved increased with the progress of the reaction time, and the generation rate on the resulting TiO_2 microspheres as well as P25 nanoparticles was ~2.32 μmol/h (TiO_2-1), ~3.85 μmol/h (TiO_2-2), ~2.01 μmol/h (TiO_2-4) and 1.58 μmol/h (P25), respectively. It is known that the recombination of photoinduced electrons and holes in a photocatalyst is a major factor that affects photocatalytic activity [32,33]. Typically, defects in the bulk semiconductor material and surface regions of the semiconductor could be the recombination centers. The high crystallinity can effectively reduce the defects. Since the resulting TiO_2 microspheres had similar crystal structures and high degrees of crystallinity, the primary drivers of hydrogen evolution was likely due to their high surface areas in combination with the dimensions of the nanorods. On the other hand, the surface microstructure of the TiO_2, and in particular, the size of TiO_2 nanorods, substantially affected the photocatalytic H_2 generation. The highly regular and considerable size of the TiO_2 nanorods, which allowed for the more efficient transfer of electrons, have proven to be an important factor in the observed robust photocatalytic activity [34,35]. The TiO_2-2 photocatalyst exhibited the largest nanorod size (~21.5 nm in length and ~11.3 nm in diameter), which would be beneficial for charge separation.

4. Conclusions

In summary, we have developed a facile, high-yield and reproducible method for the synthesis of well-knit and nanoporous anatase TiO_2 microspheres comprised of uniform TiO_2 nanorods. Critical synthesis parameters (e.g., surfactant type, P123 surfactant amount and other additives) were systematically investigated. It was found that the resulting TiO_2 microspheres possessed high stability and surface areas. The resulting TiO_2 microspheres under the optimized experimental conditions exhibited a 4.8-fold larger photocurrent and a 2.4-fold larger hydrogen generation rate in comparison to the commercial P25. The high photocatalytic activity of the synthesized TiO_2 microspheres may be attributed to: (i) the high surface area, allowing the microspheres harvest light energy more efficiently; (ii) high crystallinity, resulting in low recombination of photogenerated holes and electrons; and (iii) the uniform and highly packed nanorods, promoting the transportation of electron. The synthesis methodology developed in this study is environmental benign, and can be easily scaled up. Further, the approach for producing TiO_2 microspheres may be adopted for the fabrication of other metal oxide microspheres, having a hierarchical porous structure and high surface areas for desirable energy and environmental applications.

Acknowledgments

This work was supported by a Discovery Grant from the Natural Sciences and Engineering Research Council of Canada (NSERC). We thank Dr. P. Woo (Hitachi High-Technologies Canada Inc.) for the cross-section FE–SEM analysis. K.Y. acknowledges the Ontario Postdoctoral Fellowship. A.C. acknowledges NSERC and the Canada Foundation of Innovation (CFI) for the Canada Research Chair Award in Materials and Environmental Chemistry.

Appendix A. Supplementary data

Supplementary material related to this article can be found, in the online version, at http://dx.doi.org/10.1016/j.apcatb.2013.11.003.

References

[1] X. Chen, L. Liu, P. Yu, S. Mao, Science 331 (2011) 746–750.
[2] H. Yang, C. Sun, S. Qiao, J. Zou, G. Liu, S. Smith, H. Cheng, G. Lu, Nature 453 (2008) 638–641.
[3] S. Liu, A. Chen, Langmuir 21 (2005) 8409–8413.
[4] L. Gomathi Devi, R. Kavitha, Appl. Catal., B 140–141 (2013) 559–587.
[5] G. Wu, S. Thind, J. Wen, K. Yan, A. Chen, Appl. Catal., B 142–143 (2013) 590–597.
[6] D. Wang, H. Zhao, N. Wu, M.A. El Khakani, D. Ma, J. Phys. Chem. Lett. 1 (2010) 1030–1035.
[7] J. Li, Y. Yu, Q. Chen, J. Li, D. Xu, Cryst. Growth Des. 10 (2010) 2111–2115.
[8] W. Jiao, N. Li, L.Z. Wang, L. Wen, F. Li, G. Liu, H.M. Cheng, Chem. Commun. 49 (2013) 3461–3463.
[9] X. Han, Q. Kuang, M. Jin, Z. Xie, L. Zheng, J. Am. Chem. Soc. 131 (2009) 3152–3153.
[10] N. Sugishita, Y. Kuroda, B. Ohtani, Catal. Today 164 (2011) 391–394.
[11] B. Wu, C. Guo, N. Zheng, Z. Xie, G.D. Stucky, J. Am. Chem. Soc. 130 (2008) 17563–17567.
[12] Z. Zhang, X. Zhong, S. Liu, D. Li, M. Han, Angew. Chem. Int. Ed. 44 (2005) 3466–3470.
[13] B.D.V. Bavykin, J.M. Friedrich, F.C. Walsh, Adv. Mater. 18 (2006) 2807–2824.
[14] W. Fang, J. Zhou, J. Liu, Z. Chen, C. Yang, C. Sun, G. Qiao, J. Zou, S. Qiao, H. Yang, Chem. Eur. J. 17 (2011) 1423–1427.
[15] W. Li, J. Yang, Z. Wu, J. Wang, B. Li, S. Feng, Y. Deng, F. Zhang, D. Zhao, J. Am. Chem. Soc. 134 (2012) 11864–11867.
[16] A. Chen, P. Holt-Hindle, Chem. Rev. 110 (2010) 3767–3804.
[17] S. Ba Rawal, H.J. Kim, W.I. Lee, Appl. Catal., B 142-143 (2013) 458–464.
[18] B. Wang, H. Wu, L. Zhang, X. Lou, Angew. Chem. Int. Ed. 52 (2013) 4165–4168.
[19] H. Koo, Y.J. Kim, Y.H. Lee, W.I. Lee, K. Kim, N. Park, Adv. Mater. 20 (2008) 195–199.

[20] S. Wu, C. Mou, H. Lin, Chem. Soc. Rev. 42 (2013) 3862–4375.
[21] T. Suteewong, H. Sai, R. Hovden, D. Muller, M.S. Bradbury, S.M. Gruner, U. Wiesner, Science 340 (2013) 337–341.
[22] T. Ren, Z. Yuan, B. Su, Chem. Phys. Lett. 374 (2003) 170–175.
[23] J. Yu, W. Liu, H. Yu, Cryst. Growth Des. 8 (2008) 930–934.
[24] Y. Zhang, G. Li, Y.C. Wu, Y. Luo, L. Zhang, J. Phys. Chem. B 109 (2005) 5478–5481.
[25] K. Shiba, M. Tagaya, R.D. Tilley, N. Hanagata, Sci. Technol. Adv. Mater. 14 (2013) 023002.
[26] T. Leshuk, S. Linley, G. Baxter, F. Gu, ACS Appl. Mater. Interfaces 4 (2012) 6062–6070.
[27] E.J.W. Crossland, N. Noel, V. Sivaram, T. Leijtens, J.A. Alexander-Webber, H.J. Snaith, Nature 495 (2013) 215–219.
[28] K. Yan, G. Wu, J. Wen, A. Chen, Catal. Commun. 34 (2013) 58–63.
[29] S. Thind, G. Wu, A. Chen, Appl. Catal., B 111 (2012) 38–45.
[30] A. Purwanto, W.N. Wang, T. Ogi, I.W. Lenggoro, E. Tanabe, K. Okuyama, J. Alloys Compd. 463 (2008) 350–357.
[31] A.M. Bernhard, D. Peitz, M. Elsener, A. Wokaun, O. Kröcher, Appl. Catal., B 115–116 (2012) 129–137.
[32] T.L. Thompson, J.T. Yates, Chem. Rev. 106 (2006) 4428–4453.
[33] Y. Ma, Q. Xu, X. Zong, D. Wang, G. Wu, X. Wang, C. Li, Energy Environ. Sci. 5 (2012) 6345–6351.
[34] B. Liu, E.S. Aydil, J. Am. Chem. Soc. 131 (2009) 3985–3990.
[35] I.S. Cho, Z. Chen, A.J. Forman, D. Kim, P.M. Rao, T.F. Jaramillo, X. Zheng, Nano Lett. 11 (2011) 4978–4984.